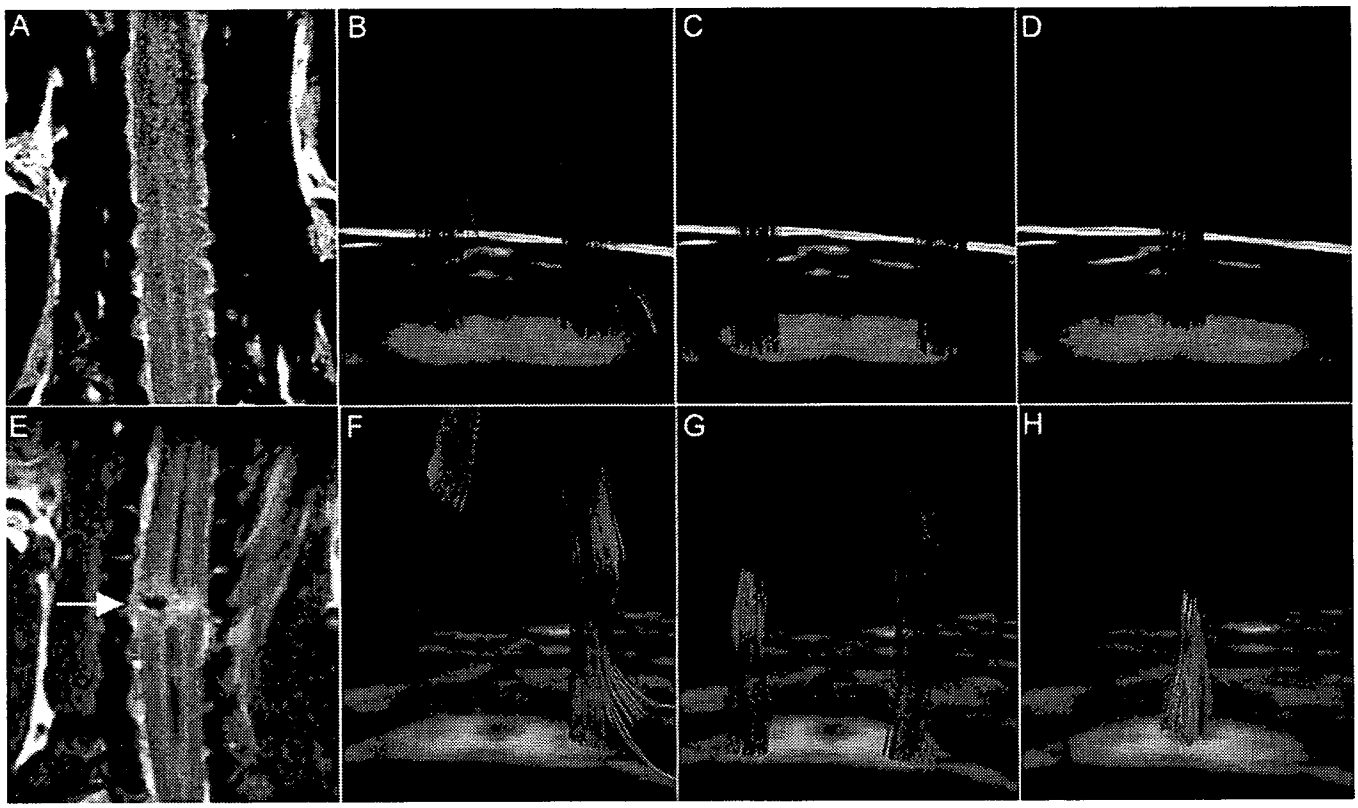

Figure 5. ***A–H***, *In vivo* pathway-specific DTT of intact and injured spinal cords in live common marmosets. MRI and tract-specific DTT of the intact spinal cord (***A–D***) and hemisected spinal cord 2 weeks after injury (***E–H***). DTTs of the CST (***B***, ***F***), spinothalamic tract (***C***, ***G***), and dorsal column-medial lemniscus pathway (***D***, ***H***) were conducted in both groups, revealing tract disruption at the hemisection site (C5/6 level) in all pathways. Although there are some limitations, pathway-specific *in vivo* DTT conducted in live animals yielded results similar to those observed in postmortem animals, especially in respect to major tract morphology.

conditions in SCI and to confirm the accuracy of DTT by comparing DTT images with histological findings, an injury with less complexity and ambiguousness was desired. With the convincing images obtained in this study, it would be interesting to examine contusion injury models in the future.

With the ability to visualize axonal projections in three-dimensions, DTT has tremendous potential as a tool to diagnose and evaluate CNS disease and trauma. In fact, DTT is already being clinically applied to visualize cerebral long tracts in cerebral surgery (Kamada et al., 2005b; Okada et al., 2006). Although there have been several preliminary studies of spinal cord DTI and DTT, they have not fully explored the potential of DTI technology. One reason DTI of the spinal cord has been less studied compared with the brain is the technical difficulty involved in conducting imaging of the spinal cord. DTI of the spinal cord requires high spatial resolution, is easily affected by magnetic susceptibility, and is obscured by *in vivo* bulk motion brought about by the beating of the heart, respiration, and the flow of CSF (Basser and Jones, 2002; Maier and Mamata, 2005; Kharbanda et al., 2006). In the present study, a 7.0 tesla MRI was used to obtain images with high resolution and a spin echo protocol was used to minimize magnetic susceptibility. To eliminate the effect of *in vivo* bulk motion, we first conducted our study using postmortem animals. Because a previous study demonstrated a degradation of diffusion anisotropy in the postmortem spinal cord (Matsuzawa et al., 1995; Madi et al., 2005), we performed all imaging immediately after animals were killed. By using postmortem animals it was possible to conduct scans of long duration (an average scan time of 10 h), resulting in images with high spatial resolution.

In our study using live animals, all animals were maintained under general anesthesia and cardiac-gated imaging was incorporated to minimize the effects of bulk motion. Under general anesthesia, marmosets were immobilized on an acrylic bed with a specially designed head positioner. Because the total scan duration was limited by anesthetic considerations, scan time (average 1.5 h) and, therefore, scan area and spatial resolution were limited compared with postmortem animal studies. However, it is of enormous importance that DTT of a live animal was able to visualize intact neural pathways and also the disrupted pathways in an injured animal, because this is the only method currently available or in development that can reveal *in vivo* axonal pathways.

In this study, we focused mainly on the CST to conduct pathway-specific DTT because it is the most important pathway in terms of motor function and often becomes the subject of scrutiny in studies of spinal cord injury treatment protocols. CST-specific DTT accurately depicted the course of the CST from the medulla to the cervical spinal cord and succeeded in imaging the "pyramidal decussation," which has been considered difficult to visualize. Furthermore, CST-specific DTT of the hemisected animal revealed the disruption of the CST at the site of injury. By using the dTV DTT software (Kunimatsu et al., 2003; Masutani et al., 2003), it is also possible to set the ROI at any point of interest and to perform voxel unit fiber tracking from that position within the threshold limit set for diffusion anisotropy. This allowed us to conduct DTT of the afferent pathways in both intact and injured spinal cords, illustrating the enormous value of this method. This capability to visualize specific projections can be applied to various studies of the spinal cord. For example, an

interesting study would be a study of ascending projections and its involvement in allodynia, using functional MRI to assess sensory dysfunction (Hofstetter et al., 2005; Lilja et al., 2006).

DTT is a new technique that traces white matter fiber trajectories by tracking the direction of faster diffusion, which is assumed to correspond to the longitudinal axis of the tract. However it is important to keep in mind that the tracking is conducted in units called voxels, which, in this study, is 0.215 mm in size, considerably larger than any one individual axonal tract. Therefore, what is actually being tracked is a group of axonal fibers with perhaps some tissue other than the intended fibers at times included in the same voxel (Mori and van Zijl, 2002; Mori and Zhang, 2006). When tissues other than the targeted axonal tract are present within the same voxel, their diffusion anisotropy interferes destructively in a phenomenon referred to as partial volume effect (Alexander et al., 2001). For example, if multiple axonal fiber tracts with different trajectories cross within the same voxel, their diffusion anisotropy becomes merged and may become more isotropic, losing directional information. The tracking procedure is often terminated because the path comes to a voxel that has lost directional orientation (anisotropy) as a result of this partial volume effect (Fig. 3*A–E*). Partial volume effect can also result in a misleading redirection of anisotropy, leading to incorrect fiber tracking. It is also important to understand that the number of tracts traced by DTT does not necessarily reflect the actual volume of white matter fiber trajectories (Fig. 3*A–E*).

With the convincing images obtained in this study, the possibilities and the limitations of spinal cord DTT need to be further explored. For example, the next step would be DTT of contusion SCI models. Another significant point that needs to be studied, is whether DTT has the sensitivity to detect regenerating axons. If confirmed, DTT would allow tracing studies at multiple time points in the same animal/patient, becoming an indispensable tool to monitor and evaluate the effectiveness of any treatment protocol for spinal cord injury. Whatever the results reveal, DTT of the spinal cord is a powerful tool with tremendous potential if its properties and limitations are fully understood and correctly applied.

References

Alexander AL, Hasan KM, Lazar M, Tsuruda JS, Parker DL (2001) Analysis of partial volume effects in diffusion-tensor MRI. Magn Reson Med 45:770–780.

Basser PJ, Jones DK (2002) Diffusion-tensor MRI: theory, experimental design and data analysis—a technical review. NMR Biomed 15:456–467.

Basser PJ, Pierpaoli C (1996) Microstructural and physiological features of tissues elucidated by quantitative-diffusion-tensor MRI. J Magn Reson B 111:209–219.

Basser PJ, Mattiello J, LeBihan D (1994) MR diffusion tensor spectroscopy and imaging. Biophys J 66:259–267.

Beaulieu C (2002) The basis of anisotropic water diffusion in the nervous system—a technical review. NMR Biomed 15:435–455.

Carpenter MB, Sutin J (1983) Human neuroanatomy, Ed 8, pp 282–289. Baltimore: Lippincott, Williams and Wilkins.

Conturo TE, Lori NF, Cull TS, Akbudak E, Snyder AZ, Shimony JS, McKinstry RC, Burton H, Raichle ME (1999) Tracking neuronal fiber pathways in the living human brain. Proc Natl Acad Sci USA 96:10422–10427.

Ducreux D, Lepeintre JF, Fillard P, Loureiro C, Tadie M, Lasjaunias P (2006) MR diffusion tensor imaging and fiber tracking in 5 spinal cord astrocytomas. AJNR Am J Neuroradiol 27:214–216.

Facon D, Ozanne A, Fillard P, Lepeintre JF, Tournoux-Facon C, Ducreux D (2005) MR diffusion tensor imaging and fiber tracking in spinal cord compression. AJNR Am J Neuroradiol 26:1587–1594.

Hofstetter CP, Holmstrom NA, Lilja JA, Schweinhardt P, Hao J, Spenger C, Wiesenfeld-Hallin Z, Kurpad SN, Frisen J, Olson L (2005) Allodynia limits the usefulness of intraspinal neural stem cell grafts; directed differentiation improves outcome. Nat Neurosci 8:346–353.

Holder CA, Muthupillai R, Mukundan Jr S, Eastwood JD, Hudgins PA (2000) Diffusion-weighted MR imaging of the normal human spinal cord *in vivo*. AJNR Am J Neuroradiol 21:1799–1806.

Ito R, Mori S, Melhem ER (2002) Diffusion tensor brain imaging and tractography. Neuroimaging Clin N Am 12:1–19.

Iwanami A, Yamane J, Katoh H, Nakamura M, Momoshima S, Ishii H, Tanioka Y, Tamaoki N, Nomura T, Toyama Y, Okano H (2005a) Establishment of graded spinal cord injury model in a nonhuman primate: the common marmoset. J Neurosci Res 80:172–181.

Iwanami A, Kaneko S, Nakamura M, Kanemura Y, Mori H, Kobayashi S, Yamasaki M, Momoshima S, Ishii H, Ando K, Tanioka Y, Tamaoki N, Nomura T, Toyama Y, Okano H (2005b) Transplantation of human neural stem cells for spinal cord injury in primates. J Neurosci Res 80:182–190.

Kamada K, Todo T, Morita A, Masutani Y, Aoki S, Ino K, Kawai K, Kirino T (2005a) Functional monitoring for visual pathway using real-time visual evoked potentials and optic-radiation tractography. Neurosurgery 57 [Suppl]:121–127.

Kamada K, Todo T, Masutani Y, Aoki S, Ino K, Takano T, Kirino T, Kawahara N, Morita A (2005b) Combined use of tractography-integrated functional neuronavigation and direct fiber stimulation. J Neurosurg 102:664–672.

Kaneko S, Iwanami A, Nakamura M, Kishino A, Kikuchi K, Shibata S, Okano HJ, Ikegami T, Moriya A, Konishi O, Nakayama C, Kumagai K, Kimura T, Sato Y, Goshima Y, Taniguchi M, Ito M, He Z, Toyama Y, Okano H (2007) A selective Sema3A inhibitor enhances regenerative responses and functional recovery of the injured spinal cord. Nat Med 12:1380–1389.

Kharbanda HS, Alsop DC, Anderson AW, Filardo G, Hackney DB (2006) Effects of cord motion on diffusion imaging of the spinal cord. Magn Reson Med 56:334–339.

Kulkarni MV, Williams JC, Yeakley JW, Andrews JL, McArdle CB, Narayana PA, Howell RR, Jonas AJ (1987) Magnetic resonance imaging in the diagnosis of the cranio-cervical manifestations of the mucopolysaccharidoses. Magn Reson Imaging 5:317–323.

Kunimatsu A, Aoki S, Masutani Y, Abe O, Mori H, Ohtomo K (2003) Three-dimensional white matter tractography by diffusion tensor imaging in ischaemic stroke involving the corticospinal tract. Neuroradiology 45:532–535.

Lacroix S, Havton LA, McKay H, Yang H, Brant A, Roberts J, Tuszynski MH (2004) Bilateral corticospinal projections arise from each motor cortex in the macaque monkey: a quantitative study. J Comp Neurol 473:147–161.

Le Bihan D, Breton E, Lallemand D, Grenier P, Cabanis E, Laval-Jeantet M (1986) MR imaging of intravoxel incoherent motions: application to diffusion and perfusion in neurologic disorders. Radiology 161:401–407.

Lee JS, Han MK, Kim SH, Kwon OK, Kim JH (2005) Fiber tracking by diffusion tensor imaging in corticospinal tract stroke: topographical correlation with clinical symptoms. NeuroImage 26:771–776.

Lemon RN, Kirkwood PA, Maier MA, Nakajima K, Nathan P (2004) Direct and indirect pathways for corticospinal control of upper limb motoneurons in the primate. Prog Brain Res 143:263–279.

Levi AD, Dancausse H, Li X, Duncan S, Horkey L, Oliviera M (2002) Peripheral nerve grafts promoting central nervous system regeneration after spinal cord injury in the primate. J Neurosurg 96:197–205.

Lilja J, Endo T, Hofstetter C, Westman E, Young J, Olson L, Spenger C (2006) Blood oxygenation level-dependent visualization of synaptic relay stations of sensory pathways along the neuroaxis in response to graded sensory stimulation of a limb. J Neurosci 26:6330–6336.

Madi S, Hasan KM, Narayana PA (2005) Diffusion tensor imaging of *in vivo* and excised rat spinal cord at 7 T with an icosahedral encoding scheme. Magn Reson Med 53:118–125.

Maier SE, Mamata H (2005) Diffusion tensor imaging of the spinal cord. Ann NY Acad Sci 1064:50–60.

Masutani Y, Aoki S, Abe O, Hayashi N, Otomo K (2003) MR diffusion tensor imaging: recent advance and new techniques for diffusion tensor visualization. Eur J Radiol 46:53–66.

Matsuzawa H, Kwee IL, Nakada T (1995) Magnetic resonance axonography of the rat spinal cord: postmortem effects. J Neurosurg 83:1023–1028.

Mori H, Masutani Y, Aoki S, Abe O, Hayashi N, Masumoto T, Yamada H, Yoshikawa T, Kunimatsu A, Ohtomo K, Kabasawa H (2003) [Simple visualization of the corticospinal pathway using tractography: one-ROI

and two-ROI methods]. Nippon Igaku Hoshasen Gakkai Zasshi 63:51–53.

Mori S, van Zijl PC (2002) Fiber tracking: principles and strategies—a technical review. NMR Biomed 15:468–480.

Mori S, Zhang J (2006) Principles of diffusion tensor imaging and its applications to basic neuroscience research. Neuron 51:527–539.

Moseley ME, Cohen Y, Kucharczyk J, Mintorovitch J, Asgari HS, Wendland MF, Tsuruda J, Norman D (1990) Diffusion-weighted MR imaging of anisotropic water diffusion in cat central nervous system. Radiology 176:439–445.

Okada T, Mikuni N, Miki Y, Kikuta K, Urayama S, Hanakawa T, Fushimi Y, Yamamoto A, Kanagaki M, Fukuyama H, Hashimoto N, Togashi K (2006) Corticospinal tract localization: integration of diffusion-tensor tractography at 3-T MR imaging with intraoperative white matter stimulation mapping—preliminary results. Radiology 240:849–857.

Olson L (2002) Med: clearing a path for nerve growth. Nature 416:589–590.

Pajevic S, Pierpaoli C (1999) Color schemes to represent the orientation of anisotropic tissues from diffusion tensor data: application to white matter fiber tract mapping in the human brain. Magn Reson Med 42:526–540.

Qiu Y, Wada Y, Otomo E, Tsukagoshi H (1991) Morphometric study of cervical anterior horn cells and pyramidal tracts in medulla oblongata and the spinal cord in patients with cerebrovascular diseases. J Neurol Sci 102:137–143.

Ralston DD, Ralston III HJ (1985) The terminations of corticospinal tract axons in the macaque monkey. J Comp Neurol 242:325–337.

Stejskal EO, Tanner JE (1965) Spin diffusion measurements: spin echoes in the presence of a time dependent field gradient. J Chem Phys 42:288–292.

Terashima T, Ochiishi T, Yamauchi T (1994) Immunohistochemical detection of calcium/calmodulin-dependent protein kinase II in the spinal cord of the rat and monkey with special reference to the corticospinal tract. J Comp Neurol 340:469–479.

Tsuchiya K, Fujikawa A, Suzuki Y (2005) Diffusion tractography of the cervical spinal cord by using parallel imaging. AJNR Am J Neuroradiol 26:398–400.

Tuszynski MH, Grill R, Jones LL, McKay HM, Blesch A (2002) Spontaneous and augmented growth of axons in the primate spinal cord: effects of local injury and nerve growth factor-secreting cell grafts. J Comp Neurol 449:88–101.

Yamashita Y, Takahashi M, Matsuno Y, Sakamoto Y, Oguni T, Sakae T, Yoshizumi K, Kim EE (1990) Chronic injuries of the spinal cord: assessment with MR imaging. Radiology 175:849–854.

3. 筋萎縮性側索硬化症のAMPA受容体仮説

東京大学大学院医学系研究科脳神経医学専攻神経内科学　日出山拓人
同　神経内科学准教授　郭　　伸

key words　ALS, AMPA receptor, GluR2, ADAR2, RNA editing

要　旨

我々のグループは，孤発性ALS脊髄運動ニューロンでは，グルタミン酸受容体であるAMPA（α-3-hydroxy-5-methyl-4-isoxazole propionic acid）受容体サブユニットの一つであるGluR2のQ/R部位にRNA編集が起こらない未編集型のGluR2増加が，疾患特異的，細胞選択的に起こっていることを見いだし，この分子変化がチャネルのCa^{2+}透過性亢進を通じて神経細胞死の直接原因になり，しかも変異SOD1関連家族性ALSを含めた他の神経変性疾患にはみられないことから，孤発性ALSの病因と考えられることを明らかにした[1]．私たちのグループの仮説の詳細は別稿を参照されたい[2,3]．本稿では，ALSのAMPA受容体仮説に至るまでの歴史的な経緯と背景を紹介する．機能分子の異常が細胞死と直結している点でこの仮説を証明することが，病因の解明のみならず特異的治療への道を切りひらく可能性があると考えている．

動　向

ALSは，1870年代にJean-Martin Charcotにより疾患概念が確立してから約140年となるが，今なお原因不明で運動ニューロンだけがある時期からなぜ突然死ぬのか，という機序は依然として解明されていない．孤発性ALSは全患者の90%以上を占め，中毒説（農薬，鉛，水銀，アルミニウム，ALSと病態の似ている南アジアや東アフリカの地方病neurolathylismとの関連が疑われているエジプト豆に含有されるβ-N-oxalylamino-L-alanine: BOAA，グアム島のALS PD dementia complexの原因とされたソテツ中のアミノ酸β-N-methylamino-L-alanine: BMAAなど），神経栄養因子欠乏説，細胞骨格タンパク異常説，逆行性軸索流異常説（dynein/dynactin）などが検討されてきたが，いずれも証明されていない．最も有力な仮説は，グルタミン酸受容体サブタイプであるAMPA受容体を介した興奮性神経細胞死仮説であり，中でも我々が見いだした孤発性ALS運動ニューロン選択的に生じているAMPA受容体のGluRサブユニットmRNAのRNA編集異常は，高い疾患特異性をもち，かつ神経細胞死の一次原因であることから孤発性ALSの病因と密接に関連すると考えられ，これを支持する知見が積み重ねられ現在に至っている．

A. 興奮性神経細胞死とは？

錐体路はグルタミン酸が神経伝達物質であり，脊髄運動ニューロンもこの興奮性入力を豊富に受

けている．そのため運動ニューロンにおいてもグルタミン酸受容体が高密度で発現しており[4]，グルタミン酸による興奮が過剰になるとCa^{2+}などのイオン透過性亢進が引き起こされ，細胞内環境の変化を補償する機能を越えてしまい，その結果として細胞死のカスケードが働く，というのが興奮性神経細胞死のメカニズムである．これは，主に虚血や低血糖，外傷，てんかん重積などの急性の神経細胞死に働くと考えられていた[5]．一方で近年，培養細胞系，*in vivo*動物実験系で急性には神経細胞死を引き起こさない濃度でも受容体が長期間持続的に興奮することで遅発性の神経細胞死が起こることが次々と明らかにされ，特にALSでグルタミン酸受容体を介した経路が関与している可能性が注目されるようになった[6,7]．

動物実験では器官培養脊髄の前角運動ニューロンにおいて培養液中にグルタミン酸トランスポーターの阻害剤を加えると変性が起こり[8]，長期間持続的にトランスポーターをコードするmRNAのアンチセンスmRNAを投与し，トランスポータータンパクの発現を抑えるとラット脊髄運動ニューロンに変性が生じた．また，ラット脊髄クモ膜下腔にグルタミン酸トランスポーター阻害剤であるTHAを投与することにより，AMPA受容体を介した遅発性の神経細胞死が後角ニューロンに生ずる[9]．これらの結果から，グルタミン酸トランスポーターの異常によりシナプス間隙のグルタミン酸濃度が上昇すると脊髄運動ニューロンが障害されることが示された．この神経細胞死はAMPA受容体アンタゴニストにより回避されるのでAMPA受容体の持続的興奮が関与していることが示されている．さらに，プライマリーカルチャーでは，脊髄前角ニューロンは後角ニューロンに比べ，AMPA受容体アゴニストに対する毒性に脆弱であること[10]，AMPA受容体アゴニストを長時間持続的にラット脊髄クモ膜下腔に投与すると後角脊髄ニューロンに遅発性の神経細胞死を起こし[11]，特にカイニン酸の4～8週間の持続投与では運動ニューロンが選択的に変性することが*in vivo*実験で示され[12]，AMPA受容体の持続的興奮により運動ニューロンに遅発性の神経細胞死が起きることが様々な実験系で示された．これらはAMPA受容体を介する神経細胞死がALSの神経細胞死に働いていることを示唆するものである[2,3]．

B. 神経細胞死とAMPA受容体

グルタミン酸受容体は大きくイオンチャネル型と代謝調節型に分類される．そしてイオンチャネル型はさらにNMDA受容体，カイニン酸受容体，AMPA受容体に分けられる．NMDA受容体が急性の神経細胞死に関与するのに対して特に速いシナプス伝達にかかわるAMPA受容体は，ニューロンの遅発性の細胞死に関与し，運動ニューロンは，特に後者の興奮性細胞死に脆弱であることが知られている．その分子メカニズムとして細胞死に先立つ過剰なCa^{2+}流入による細胞内Ca^{2+}濃度の持続的上昇が培養ニューロンで明らかにされ，それに引き続くCa^{2+}依存性プロテアーゼの活性化，ミトコンドリア障害，NOS産生などによるカスケードが細胞死を引き起こすことが様々な実験系により明らかにされた[13]．神経細胞内Ca^{2+}濃度上昇の機構には，1）NMDA受容体の活性化によるチャネルからのCa^{2+}流入，2）Ca^{2+}透過性AMPA受容体の活性化，3）代謝型グルタミン酸受容体などの興奮によるIP3産生を介する小胞体からのCa^{2+}動員，4）膜の脱分極による膜電位依存性Ca^{2+}チャネルの開口などのメカニズムが知られている[14]．最近は電位非依存性カチオン透過性チャネルの関与も示唆されている（例：transient receptor potential，以下TRP）[15]．なぜ神経細胞死にAMPA受容体のCa^{2+}透過性の関与が大きいのか，についてはまだ不明な点が多い

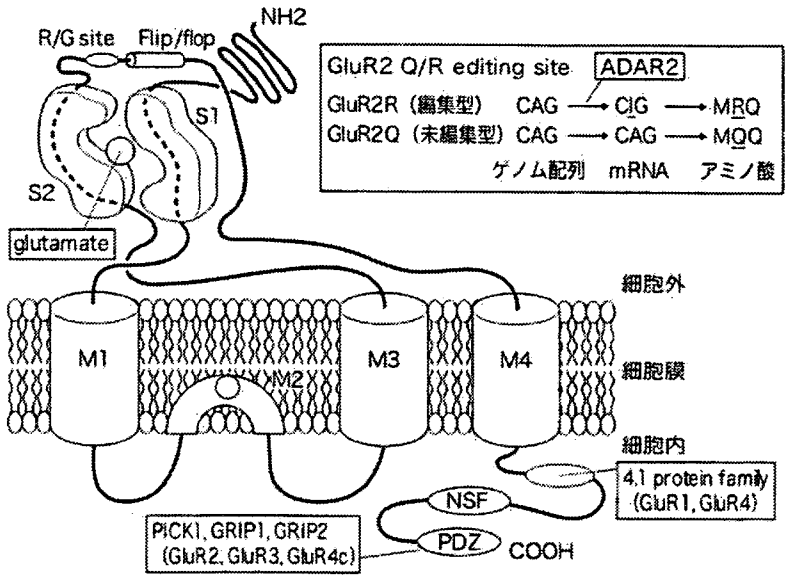

図1　AMPA受容体の構造（文献2,3,16-20より改変）

AMPA受容体は4種類のサブユニットGluR1～GluR4から構成される4量体からなる．M1～M4は膜ドメイン．S1とS2は仮想的グルタミン酸結合部位．各サブユニットにはそれぞれ選択的スプライシングにより異なるアミノ酸配列をもったflip型とflop型という2つのタイプがあり，発生時期や脳の部位で異なっている．GluR2～4にはR/G部位があり，RNA編集によりアルギニン（R）からグリシン（G）へ置換する．この部位は受容体脱感作を修飾する．さらにGluR2の多様性が生じるメカニズムとしてM2に存在するQ/R編集部位があり，翻訳過程でCAGまたはCAA（グルタミン（Q））がCGGまたはCGA（アルギニン（R））になる．そのため，サブユニットの組み合わせの違いが機能的な多様性をもたらすと推測される．細胞内C末端領域にはPKA，PKC，CaMKIIによるリン酸化部位やGRIP，PICK，SAP97などのPDZタンパク質結合部位が局在する．この領域はPDZドメインを介してGRIPなどpostsynaptic density（PSD）タンパクと結合し，シナプスでのAMPA受容体の安定化などにかかわっている．また，AMPA受容体はTARPタンパク（本文参照），stargazinタンパク（VDCC γ2），VDCC γ3-8と膜表面で共在することが知られており，これらのタンパクがチャネル活性とかかわっていることがわかっている．

PDZ: Postsynaptic density-95/Discs large/Zona occuludens-1,
PKA: protein kinase A, PKC: protein kinase A,
CaMKII: Ca^{2+}/ calmodulin-dependent protein kinase phosphates II, GRIP1: glutamate receptor-interacting protein type 1, GRIP2: glutamate receptor-interacting protein type 2,
PICK: protein that interacts with C kinase, SAP97: synapse-associated protein 97,
NSF: N-ethylmaleamide sensitive factor, PSD: postsynapitic density,
VDCC: voltage-dependent Ca^{2+} channel
図中のCIGは，リボソームでIはグアノシン（G）と同等であると見なされるため，CIGというコドンはCGGと見なされRとして翻訳される（本文参照）．

が，どのようにCa^{2+}透過性が制御されているかは少しずつ解明されている．

AMPA受容体は，4種のサブユニット（GluR1-GluR4）の単独または様々な組み合わせからなる4量体である．各サブユニットは共通構造をもち，相互に約70%のアミノ酸配列の相同性をもち，細胞外のN端，膜ドメイン（M1～M4），細胞内のC端からなる（図1）[2,3,16-20]．AMPA受容体

のCa^{2+}透過性を決定する因子には，1) GluR2サブユニット，2) GluR2サブユニットのRNA編集（特にQ/R部位），3) flip/flop splicing variantやR/G部位の編集率などチャネルの開口を編集するドメインがあり，細胞全体としては[4]細胞表面のAMPA受容体密度もCa^{2+}流入量を決定する大きな因子となる．しかし，これらの因子のすべてが細胞死に直接関連するわけではなく，AMPA受容体仮説には後述するように1)と2)のかかわりが大きい．

第一にチャネルのCa^{2+}透過性決定に重要な役割をはたしているのはGluR2サブユニットである．AMPA受容体を構成する4つのサブユニットのうちGluR2を含む受容体は，Ca^{2+}透過性が低く，GluR2を含まないGluR1，3，4のサブユニットだけで構成された受容体は，高いCa^{2+}透過性を示す[21-23]．

つまりAMPA受容体のCa^{2+}透過性は，GluR2の有無により決定される．たとえば，ラット小脳プルキニエ細胞や海馬錐体細胞などでは，他のサブユニットに比べGluR2が多く発現し，AMPA受容体のCa^{2+}透過性は低く[24]，海馬のバスケット細胞，新皮質の非錐体細胞，小脳のBergmannグリア細胞などではGluR2サブユニットがほとんど発現していないため，Ca^{2+}透過性は高い[25]ことが知られている．

第二にAMPA受容体の各サブユニットのM2にあるQ/R部位がCa^{2+}透過性を制御している．Q/R部位がCa^{2+}透過性決定に重要なのはチャネル・ポアに面しており，陽電化のRがCa^{2+}を弾くのに対して電気的に中性のQではこの作用が弱いためであると考えられている．同部位はGluR2以外ではグルタミン（Q）であるのに対して，GluR2だけはアルギニン（R）である（図1）．しかしゲノムレベルでは，GluR2も他のサブユニット同様にQをコードしている．どうしてRになるのかというと，RNA編集という現象が起こるためである．つまり，DNAからRNAへ転写後，mRNAになる前に，adenosine deaminase acting on RNA type 2（以下ADAR2）とよばれる編集酵素により，アデノシン（A）からイノシン（I）へとRNA編集が起こることで塩基置換され，リボソームでIはグアノシン（G）と同等であると見なされるため，CIGというコドンはCGGと見なされRとして翻訳される[26]．未編集型GluR2（Q）は他のサブユニット同様AMPA受容体のCa^{2+}透過性を制御できないので，編集型GluR2（R）を含んだAMPA受容体の割合が減少する，あるいは未編集型GluR2（Q）を含んだAMPA受容体の割合が増加すると細胞内へのCa^{2+}流入が高まる[27]．RNA編集は，GluR2 Q/R部位以外にもカイニン酸受容体サブユニットであるGluR5，GluR6のQ/R部位やGluR2，GluR3，GluR4サブユニットのR/G部位，Kv1.1 I/V部位，$5HT_{2c}$ A～E部位ではRNA編集の有無によりチャネル特性に変化が生じ，ADAR2のself-editingではスプライシングサイトの変化によるフレームシフトにより，酵素活性が変化する[28]など様々なRNAのそれも複数の部位で生じているが，その編集率は一定せず様々である．ところが，GluR2のQ/R部位は，胎生期から成熟期に至るまでほぼ100%編集されている[29]という点で特異的であり，他には見いだされていない．

しかし，GluR2のノックアウトマウスでは細胞死が生じず[30]，一方でRNA編集を阻止したmutant mouseはGluR2 Q/R部位が0.1%以下に低下し，生後20日以内に痙攣重積により死亡する[31]ことなどからGluR2のRNA編集にはQ/R部位の電荷状態の制御以外にも，AMPA受容体の機能を修飾する作用があると考えられ，生存を左右するほど生物学的にもきわめて重要な意味をもっていると推測される．

その修飾作用の一つが，ニューロン表面のAMPA受容体密度，サブユニット会合効率への

関与である．GregerらはQ/R部位がQかRであるかによってサブユニットの会合確率が変わり，特に4量体形成において主な要因となること，すなわち，未編集型GluR2（Q）は編集型GluR2（R）よりも効率的に機能的AMPA受容体を形成しやすいことを示した[32]．さらにQ/R部位のアミノ酸残基の違いによりtrafficking効率が異なり，Q型（GluR1, 3, 4, 未編集GluR2（Q））はR型（編集型GluR2（R））に比し効率が高いこと，すなわち未編集型GluR2（Q）が存在する場合には編集型GluR2（R）が小胞体から輸送されにくいのに対して，GluR2（Q）を含むサブユニット複合体は，効率よく膜表面にtraffickingされることを示した[33]．以上のようにQ/R部位がQであるかRであるかによってサブユニットの会合確率およびtrafficking効率が異なり，結果的にGluR2の細胞膜表面へのtrafficking効率は，編集型GluR2（R）より未編集型GluR2（Q）のほうがはるかに高くなる．すなわち，GluR2ノックアウトマウスには細胞死が起こらないのに，RNA編集異常マウスで痙攣重積が起こるのは，RNA編集の障害の方が細胞表面のCa^{2+}透過性AMPA受容体密度が高く，細胞内Ca^{2+}濃度の上昇もより大きいので神経細胞死が起こると考えられる．培養細胞では，未編集型GluR2発現させても，traffickingを阻止すると神経細胞死も阻止される[34]．

C. AMPA受容体サブユニット発現とALSの運動ニューロン死

これらの結果を踏まえ，神経細胞死に関連する分子変化であるGluR2の減少（Ca^{2+}透過性AMPA受容体の割合の増加）ないしGluR2 Q/R部位の編集率低下（Ca^{2+}透過性AMPA受容体の実質的増加）の有無をALSの運動ニューロンで検討するためにKwakらはlaser microdissectorを用いて凍結割検組織から単一神経細胞を切り出し，孤発性ALS脊髄運動ニューロンの単一神経細胞レベルの検討において，GluR2 mRNA発現量に有意な減少がないこと[35]，および脊髄前角組織レベルで，すでに報告していた[36]部位選択的・疾患特異的なGluR2 Q/R部位の編集率低下を確認した[1]．図2に示すように，正常対照群の運動ニューロンでは，全例GluR2 Q/R部位は100% RNA編集されていたが，ALS群では0～100%とばらつき，平均値は38～75%と低下していた．ALS群における小脳プルキンエ細胞の編集率は，正常対照群と同様にほぼ100%に保たれていた．また，他の神経変性疾患の同細胞を検索したが，編集率は正常対照と同様のレベルによく保たれていた．さらに症例数を増やし，孤発性ALSと診断された症例で，古典型，PBP，ALS-D，好塩基性封入体が出現する若年発症例[37]について編集率を調べたところ臨床像の異なるこれらのALSでも編集率は低下しており，共通の分子異常が発症のメカニズムにあることが推測される[38]．一方でSOD1関連性家族性ALS（ALS1）モデルラットやSBMA（球脊髄性筋萎縮症）の運動ニューロンでは同部位の編集率はコントロールと同様であり[39]，これらの疾患の運動ニューロンでは孤発性ALSとは異なる細胞死のメカニズムが働いていると考えられる．一方で，変異*SOD1*トランスジェニックマウスでは，AMPA受容体を介した神経細胞死が働いていることが，GluR2欠損マウスとの交配による興奮毒性の増強[40]やCa^{2+}を透過するQ/R部位を人工的なGluR2〔GluR-B（N），N（アスパラギン）〕を導入した変異マウスと変異*SOD1*遺伝子のdouble transgenicマウスにおける神経細胞死の促進[41]から示されている．ALS1でGluR2のRNA編集が正常だとすると，GluR2の欠乏によるAMPA受容体のCa^{2+}透過性亢進が予想されるが，GluR2の過剰発現により生存期間が延長することを示した報告[42]，GluR3の発現量が増加しているとする

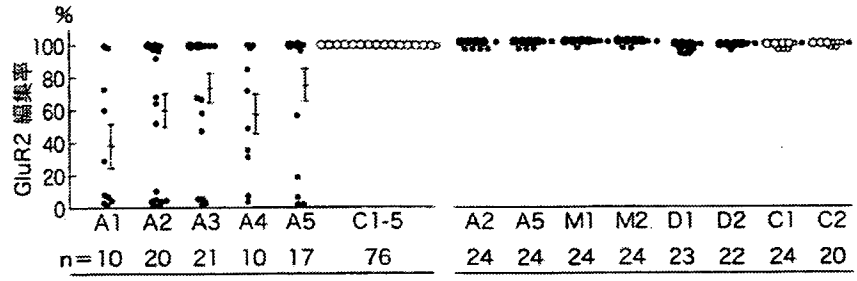

図2　単一神経細胞におけるGluR2 Q/R部位RNA編集率（文献1より改変）
各点（大きな点は5細胞，小さな点は1細胞）は，ALS群5例（A1-A5），コントロール群5例（C1-C5）の単一脊髄運動ニューロンにおけるGluR2 Q/R部位のRNA編集率と，ALS群2例（A2，A5），multiple system atrophy（以下MSA，多系統萎縮症）群2例（M1，M2），dentatorubral-pallidoluysian atrophy（以下DRPLA，歯状核赤核淡蒼球ルイ体萎縮症）群2例（D1，D2），コントロール群2例（C1，C2）の単一小脳プルキンエ細胞の編集率を表している．平均値± 標準誤差と解析した細胞数（n）も示した．運動ニューロンにおける正常コントロール76個の内訳は，C1; 28，C2; 12，C3; 13，C4; 12，C5; 11である．運動ニューロンでは，正常コントロール群のすべての細胞において，例外なく編集率は100%であった．これに対して，ALS群では，解析した5ケースすべてにおいて，編集率は運動ニューロンごとに0%から100%まで大きくばらつき，平均値も正常コントロール群と比較し，有意に低下していた（Mann-Whitney U test，$p<0.001$）．一方，小脳プルキンエ細胞における編集率については，ALS群，MSA群，DRPLA群とコントロール群の間には有意差はない（Mann-Whitney U-test，$p>0.05$）．

報告[43,44]は，この予測を支持する．特に，GluR3の発現量増加は，我々がカイニン酸を長期髄注することにより作成したALSのモデルラットにもみられる分子変化であり[45]，変異SOD1トランスジェニックマウス，家族性ALS1ではAMPA受容体の持続的刺激により運動ニューロンの興奮性が高まった結果，相対的にGluR2の割合が下がることでAMPA受容体のCa^{2+}透過性が亢進し，細胞死に至るカスケードにつながることが予想される．このように，ALS1と，痴呆を伴うALSを含む孤発性ALSとでは，神経細胞死を引き起こす分子メカニズムが異なることは，ALS，前頭側頭型痴呆（FTLD）の細胞内封入体に特異的に集積することが示されているTDP-43が，ALS1には見いだされていない[46,47]ことからきわめて興味深い．他方，アンドロゲン受容体のCAGリピートが伸長しているSBMAでは，同じポリグルタミン病であるHuntington病モデルマウスでの検討から[48-51]，AMPA受容体を介した神経細胞死は働いていないと考えられる．このように運動ニューロン疾患の神経細胞死には図3に示すように，異なる複数の分子メカニズムが独立に働き，ALSにはAMPA受容体を介する運動ニューロン死が働いているものの単一の分子メカニズムではないことが推測される[52]．

以上から，孤発性ALS脊髄運動ニューロンで認められたRNA編集異常は，細胞選択的かつ疾患特異的な分子変化であり，神経細胞死に直接かかわっている可能性が高いと考えられる．このような選択性・特異性を生む機序としては，脊髄運動ニューロンのAMPA受容体総mRNA発現量およびGluR2サブユニットのAMPA受容体サブユ

ニット全体に占める比率が，他のニューロンに比べて，低く[35,53]，もともとCa^{2+}透過性AMPA受容体の割合が多いためにRNA編集低下の影響を受けやすいことがあげられる．また，これまでのADAR2ノックアウトマウスの研究から，ADAR2活低下がGluR2 Q/R部位の編集異常を通じて神経細胞死の直接原因になり得ること[54]が明らかにされている．ADAR2活性を規定する因子の一つはmRNA発現レベルであり[55,56]，孤発性ALS前角組織では正常対照に比し，ADAR2mRNA発現量が低く[16]，ALS脊髄運動ニューロンではADAR2の酵素活性が低下していることがGluR2 Q/R部位RNA編集異常の原因と考えた．この仮説を証明するために，私たちのグループはADAR2の解析を進めている．

D. ALSの治療に向けて

前述のように孤発性ALSの疾患病態と直接かかわっていると考えられるAMPA受容体関連の分子異常が見つかり，発症メカニズムに基づいた分子標的治療法を開発できる可能性が高まってきた．運動ニューロン選択的にGluR2 Q/R部位のRNA編集を回復できれば，ALSの治療へとつながるものと考えられる．我々は前述の仮説に合致する事実を次々と明らかにしているが，なぜALS

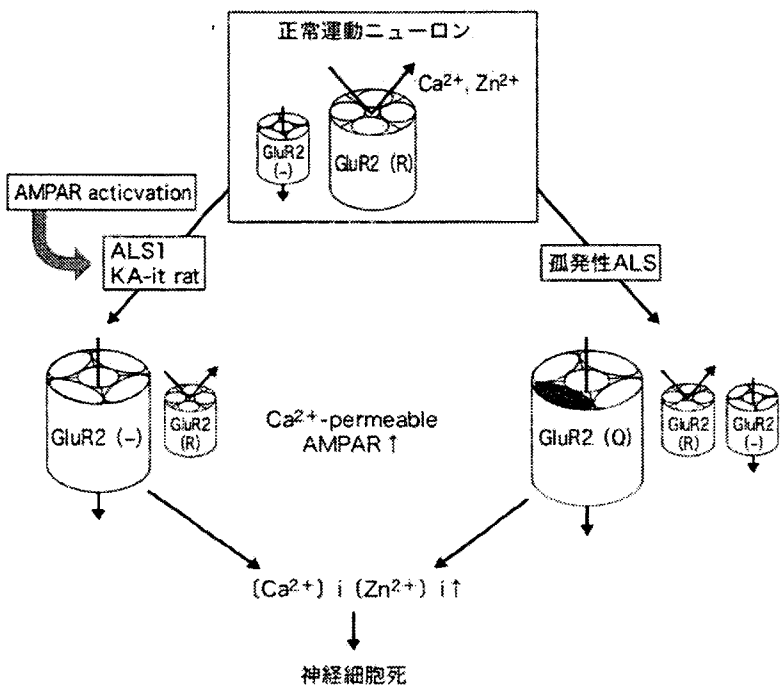

図3　AMPA受容体を介する運動ニューロンの神経細胞死の機序のまとめ（文献52を改変）
正常運動ニューロンではほとんどのAMPA受容体（AMPAR）は編集型GluR2（R）でありCa^{2+}を通さない．わずかながら運動ニューロンでGluR2を含まないCa^{2+}透過性の高いAMPARが存在することが知られている．本文中で述べたように孤発性ALS，ALS1のいずれにもAMPARを介した細胞死のメカニズムのエビデンスがあるが，両者のメカニズムは異なっている．孤発性ALSでは未編集型GluR2（Q）が増加することで透過性AMPARが増加し，一方でALS1ではGluR2の割合の減少により編集型GluR2を含まないAMPA受容体の割合が増加することで細胞内Ca^{2+}濃度が上昇し，神経細胞死が引き起こされる．ただし，前者が単独で神経細胞死が生じるのに対して，後者はSOD1の細胞毒性などの因子が加わる必要がある．

の運動ニューロンで選択的にADAR2活性が低下するのかを含め孤発性ALSの病態メカニズム解明が治療に結びつけられる成果が期待される.

文献

1) Kawahara Y, Ito K, Sun H, et al. RNA editing and death of motor neurons. Nature. 2004; 427: 801.
2) 日出山拓人, 河原行郎, 郭　伸. ALSとAMPA受容体. 脳神経. 2005; 57: 585-98.
3) 郭　伸. ALSの運動ニューロン死とグルタミン酸受容体の分子変化. 神経進歩. 2006; 50(60): 902-11.
4) 五嶋義郎. グルタミン酸受容体の歴史とその背景. Clin Neurosci. 2006; 24(2): 142-4.
5) Rothman SM, Olney JW. Glutamate and the pathophysiology of hypoxic-ischemic brain damage. Ann Neurol. 1986; 19: 105-11.
6) 相澤仁志, 中村良司, 郭　伸. 実験的遅発性興奮性運動ニューロン死. Clin Neurosci. 1998; 16(8): 58-62.
7) 郭　伸. 興奮性アミノ酸と神経障害―神経疾患の実験動物モデル. In: 後藤文男, 他, 編. AnnaulReview神経 1992. 東京: 中外医学社; 1992. p. 15-30.
8) Rothstein JD, Jin L, Dykes-Hoberg M, et al. Chronic inhibition of glutamate uptake produces a model of slow neurotoxicity. Proc. Natl Acad Sci U S A. 1993; 90: 6591-5.
9) Hirata A, Nakamura R, Kwak S, et al. AMPA receptor-mediated slow neuronal death in the rat spinal cord induced by long-term blockade of glutamate transporters with THA. Brain Res. 1997; 771: 37-44.
10) Carriedo SG, Yin HZ, Weiss JH. Motor neurons are selectively vulnerable to AMPA/kainite receptor-mediated injury in vitro. J Neurosci. 1996; 16: 4069-79.
11) Nakamura R, Kamakura K, Kwak S. Late-onset selective neuronal damage in the rat spinal cord induced by continuous intrathecal administration of AMPA. Brain Research. 1994; 654: 279-85.
12) Sun H, Kawahara Y, Ito K, et al. Slow and selective death of spinal motor neurons in vivo by intrathecal infusion of kainic acid: implications for AMPA receptor-mediated excitotoxicity in ALS. J Neurochem. 2006; 98: 782-91.
13) 鈴木岳之, 都築馨介, 亀山仁彦, 他. AMPA受容体の生理機能-受容体機能発現から疾患まで-日薬理誌. 2003; 122: 515-26.
14) 小澤瀞司. 中枢神経系のグルタミン酸受容体. 脳神経. 2001; 53: 605-15.
15) Vennekens R, Voets T, Bindels RJ, et al. Current understanding of mammalian TRP homologues. Cell Calcium. 2002; 31: 253-64.
16) Kawahara Y, Kwak S. Excitatotoxicity and ALS: What is unique about the AMPA receptors expressed on spinal motor neurons ? Amyotrophic lateral sclerosis. 2005; 1-14.
17) 日出山拓人, 河原行郎, 郭　伸. 筋萎縮性側索硬化症の分子病理～病態と治療～. 最新医学. 2005; 60(5): 1072-82.
18) 日出山拓人, 河原行郎, 郭　伸. 筋萎縮性側索硬化症の研究の進歩. 医学のあゆみ. 2005; 212(10): 2613-20.
19) Kwak S, Kawahara Y. Deficient RNA editing of GluR2 and neuronal death in ALS. J Mol Med. 2005; 83: 110-20.
20) 崎村建司. AMPA型グルタミン酸受容体の構造と機能. Clin Neurosci. 2006; 24(2): 145-8.
21) Hollmann M, Hartley M, Heinemann S. Ca^{2+} permeability of KA-AMPA--gated glutamate receptor channels depends on subunit composition. Science. 1991; 252: 851-3.
22) Verdoorn TA, Burnashev N, Monyer H, et al. Structural determinants of ion flow through recombinant glutamate receptor channels. Science. 1991; 252: 1715-8.
23) Burnashev N, Khodorova A, Jonas P, et al. Calcium-permeable AMPA-kainate receptors in fusiform cerebellar glial cells. Science. 1992; 256: 1566-70.
24) Nutt S, Kamboj R. Differential RNA editing efficiency of AMPA receptor subunit GluR-2 in human brain. Neuroreport. 1994; 5: 1679-83.
25) Geiger JR, Melcher T, Koh DS, et al. Relative abundance of subunit mRNAs determines gating and Ca^{2+} permeability of AMPA receptors in principal neurons and interneurons in rat CNS. Neuron. 1995; 15: 193-204.
26) Higuchi M, Single FN, Kohler M, et al. RNA editing of AMPA receptor subunit GluR-B: a base-paired intron-exon structure determines position and efficiency. Cell. 1993; 75: 1361-70.
27) Sommer B, Köhler M, Sprengel R, et al. RNA editing in brain controls a determinant of ion

flow in glutamate-gated channels. Cell. 2001; 67: 11-9.
28) Rueter SM, Dawson TR, Emeson RB. Regulation of alternative splicing by RNA editing. Nature. 1999; 399: 75-80.
29) Koh DS, Burnashev N, Jonas P. Block of native Ca^{2+}-permeable AMPA receptors in rat brain by intracellular polyamines generates double rectification. J Physiol. 1995; 486: 305-12.
30) Jia Z, Agopyan N, Miu P, et al. Enhanced LTP in mice deficient in the AMPA receptor GluR2. Neuron. 1996; 17: 945-56.
31) Brusa R, Zimmermann F, Koh DS, et al. Early-onset epilepsy and postnatal lethality associated with an editing-deficient Glu R-B allele in mice. Science. 1995; 270: 1677-80.
32) Greger IH, Khatri L, Kong X, et al. AMPA receptor tetramerization is mediated by Q/R editing. Neuron. 2003; 40(4): 763-74.
33) Greger IH, Khatri L, Ziff EB. RNA editing at arg607 controls AMPA receptor exit from the endoplasmic reticulum. Neuron. 2002; 34(5): 759-72.
34) Mahajan SS, Ziff EB. Novel toxicity of the unedited GluR2 AMPA receptor subunit dependent on surface trafficking and increased Ca^{2+}-permeability. Mol Cell Neurosci. 2007; 35: 470-81.
35) Kawahara Y, Kwak S, Sun H, et al. Human spinal mononeurons express low relative abundance of GluR2 mRNA: an implication for excitotoxicity in ALS. J Neurochem. 2003; 85: 680-9.
36) Takuma H, Kwak S, Yoshizawa T, et al. Reduction of GluR2 RNA editing, a molecular change that increases calcium influx through AMPA receptors, selective in the spinal ventral gray of patients with amyotrophic lateral sclerosis. Ann Neurol. 1999; 46: 806-15.
37) Aizawa H, Kimura T, Hashimoto K, et al. Basophilic cytoplasmic inclusions in a case of sporadic juvenile amyotrophic lateral sclerosis. J Neurol Sci. 2000; 176: 106-13.
38) 郭　伸, 日出山拓人, 西本祥仁, 他. 孤発性ALSの脊髄前角におけるRNA編集異常と病型. 厚生労働科学研究費補助金難治性疾患克服研究事業神経変性疾患に関する調査研究班報告書. 2007. p. 64-5.
39) Kawahara Y, Sun H, Ito K, et al. Underediting of GluR2 mRNA, a neuronal death inducing molecular change in sporadic ALS, does not occur in motor neurons in ALS1 or SBMA. Neurosci Res. 2006; 54: 11-4.
40) Van Damme P, Braeken G, Callewaert G, et al. GluR2 deficiency accelerates motor neuron degeneration in a mouse model of amyotrophic lateral sclerosis. J Neuropathol Exp Neurol. 2005; 64: 605-12.
41) Kuner R, Groom AJ, Bresink I, et al. Late-onset motoneuron disease caused by a functionally modeified AMPA receptor subunit. Proc Natl Acad Sci U S A. 2005; 102: 5826-31.
42) Tateno M, Sadakata H, Tanaka M, et al. Calcium-permeable AMPA receptors promote misfolding of mutant SOD1 protein and development of amyotrophic lateral sclerosis in a transgenic mouse model. Hum Mol Genet. 22004; 13: 2183-96.
43) Spalloni A, Albo F, Ferrari F, et al. Cu/Zn-superoxide dismutase(GLY93-->ALA) mutation alters AMPA receptor subunit expression and function and potentiates kainite-mediated toxicity in motor neurons in culture. Neurobiol Dis. 2004; 15: 340-50.
44) Tortarolo M, Grignaschi G, Calvaresi N, et al. Glutamate AMPA receptors change in motor neurons of SOD1G93A transgenic mice and their inhibition by a noncompetitive antagonist ameliorates the progression of amyotrophic lateral sclerosis-like disease. J Neurosci Res. 2006; 83: 134-46.
45) Sun H, Kawahara Y, Ito K, et al. Slow and selective death of spinal motor neurons *in vivo* by intrathecal infusion of kainic acid: implications for AMPA receptor-mediated excitotoxicity in ALS. J Neurochem. 2006; 98: 782-91.
46) Mackenzie IR, Bigio EH, Ince PG, et al. Pathological TDP-43 distinguishes sporadic amyotrophic lateral sclerosis from amyotrophic lateral sclerosis with SOD1 mutations. Ann Neurol. 2007; 61: 427-34.
47) Tan CF, Eguchi H, Tagawa A, et al. TDP-43 immunoreactivity in neuronal inclusions in familial amyotrophic lateral sclerosis with or without SOD1 gene mutation. Acta Neuropathol. 2007; 113: 535-42.

48) Levine MS, Klapstein GJ, Koppel A, et al. Enhanced sensitivity of N-methyl-D-aspartate receptor activation in transgenic and knockin mouse models of Huntington's disease. J Neurosci Res. 1999; 58: 515-32.
49) Morton AJ, Leavens W. Mice transgenic for the human Huntington's disasese mutation have reduced sensitivity to kainic acid toxicity. Brain Res Bull. 2006; 52: 51-9.
50) Snider BJ, Moss JL, Revilla FJ, et al. Neocortical neurons cultured from mice with expanded CAG repeats in the huntingtin gene: unaltered vulnerability to excitotoxins and other insults. Neuroscience. 2003; 120: 617-25.
51) Zeron MM, Hansson O, Chen N, et al. Increased sensitivity to N-methyl-D-aspartate receptor-mediated excitotoxicity in a mouse model of Huntington's disease. Neuron. 2002; 33: 849-60.
52) Kwak S, Weiss JH. Calcium-permeable AMPA channel in neurodegenerative disease and ischemia. Curr Opin Neurobiol. 2006; 16: 281-7.
53) Sun H, Kawahara Y, Ito K, et al. Expression profile of AMPA receptor subunit mRNA in single adult rat brain and spinal cord neurons in situ. Neurosci Res. 2005; 52: 228-34.
54) Higuchi M, Maas S, Single FN, et al. Point mutation in an AMPA recepotor gene rescues lethality in mice deficient in the RNA-editing enzyme ADAR2. Nature. 2000; 406: 78-81.
55) Kawahara Y, Ito K, Sun H, et al. Regulation of glutamate receptor RNA editing and ADAR mRNA expression in developing human normal and Down's syndrome brains. Dev Brain Res. 2004; 148: 151-5.
56) Kawahara Y, Ito K, Sun H, et al. Low editing efficiency of GluR2 mRNA is associated with a low relative abundant of ADAR2 mRNA in white matter of normal human brain. Eur J Neurosci. 2003; 18: 23-33.

Journal of Neurochemistry, 2007, **102**, 1497–1505 doi:10.1111/j.1471-4159.2007.04534.x

Heat-shock protein 105 interacts with and suppresses aggregation of mutant Cu/Zn superoxide dismutase: clues to a possible strategy for treating ALS

Hirofumi Yamashita,*,† Jun Kawamata,* Katsuya Okawa,‡ Rie Kanki,* Tomoki Nakamizo,* Takumi Hatayama,§ Koji Yamanaka,† Ryosuke Takahashi* and Shun Shimohama*,¶

**Department of Neurology, Kyoto University Graduate School of Medicine, Kyoto, Japan*

†Yamanaka Research Unit, RIKEN Brain Science Institute, Wako, Japan

‡Horizontal Medical Research Organization, Kyoto University Graduate School of Medicine, Kyoto, Japan

§Department of Biochemistry, Kyoto Pharmaceutical University, Kyoto, Japan

¶Department of Neurology, Sapporo Medical University School of Medicine, Sapporo, Japan

Abstract

A dominant mutation in the gene for copper-zinc superoxide dismutase (SOD1) is the most frequent cause of the inherited form of amyotrophic lateral sclerosis. Mutant SOD1 provokes progressive degeneration of motor neurons by an unidentified acquired toxicity. Exploiting both affinity purification and mass spectrometry, we identified a novel interaction between heat-shock protein 105 (Hsp105) and mutant SOD1. We detected this interaction both in spinal cord extracts of mutant $SOD1^{G93A}$ transgenic mice and in cultured neuroblastoma cells. Expression of Hsp105, which is found in mouse motor neurons, was depressed in the spinal cords of $SOD1^{G93A}$ mice as disease progressed, while levels of expression of two other heat-shock proteins, Hsp70 and Hsp27, were elevated. Moreover, Hsp105 suppressed the formation of mutant SOD1-containing aggregates in cultured cells. These results suggest that techniques that raise levels of Hsp105 might be promising tools for alleviation of the mutant SOD1 toxicity.

Keywords: amyotrophic lateral sclerosis, Cu/Zn superoxide dismutase (or superoxide dismutase 1), heat-shock protein 105.

J. Neurochem. (2007) **102**, 1497–1505.

Amyotrophic lateral sclerosis (ALS) is an adult-onset neurodegenerative disease causing the selective loss of motor neurons, which results in progressive and ultimately fatal paralysis of skeletal muscles. Death usually occurs within 2–5 years after onset of the disease and is related to respiratory-muscle weakness. Ten percent of cases of ALS are inherited, and the most frequent cause of inherited ALS is dominant mutations in the gene for Cu/Zn superoxide dismutase (SOD1). More than 100 different mutations in SOD1 have been identified, all of which provoke uniform disease phenotype that is similar to the phenotype of the sporadic disease. Transgenic mice and rats expressing a mutant human gene for SOD1 develop an ALS phenotype, although deletion of SOD1 from mice does not cause motor neuron disease, providing evidence for acquired toxicity due to mutant SOD1 (Bendotti and Carri 2004; Bruijn *et al.* 2004).

Several hypotheses have been proposed to explain the mechanism of mutant SOD1-mediated toxicity, including formation of protein aggregates due to reduced conformational stability, mitochondrial dysfunction, excitotoxicity, abnormal axonal transport, mutant-derived oxidative damage, lack of growth factors, and inflammation. However, the exact mechanism responsible for motor neuron degeneration remains unknown. One plausible hypothesis is linked to the

Received November 30, 2006; revised manuscript received February 08, 2007; accepted February 14, 2007.

Address correspondence and reprint requests to Dr Shun Shimohama, Department of Neurology, Sapporo Medical University School of Medicine, S1 W16, Chuo-ku, Sapporo 060-8543, Japan.
E-mail: shimoha@sapmed.ac.jp

Abbreviations used: ALS, amyotrophic lateral sclerosis; HRP, horseradish peroxidase; HEK, human embryonic kidney; HSF, heat shock factor; IP, immunoprecipitation; MALDI-TOF, matrix-assisted laser desorption/ionization time-of-flight; MS, mass spectrometry; PBS, phosphate-buffered saline; SDS–PAGE, sodium dodecyl sulfate–polyacrylamide gel electrophoresis; SOD, superoxide dismutase; WT, wild-type.

© 2007 The Authors
Journal Compilation © 2007 International Society for Neurochemistry,

impairment of protein-quality control. Accumulation of mutant SOD1 might result in (i) saturation of the protein-folding and protein-degradation machinery that handles mutant proteins and/or (ii) disruption of vital intracellular processes by misfolded, oligomeric species of SOD1. In such cases, it is likely that mutant SOD1 might provoke toxicity through abnormal interactions between mutant SOD1 and other proteins. In this context, identification of proteins that interact with mutant SOD1 might provide clues to the toxic effects of the mutant protein. Mutant but not wild-type (WT) SOD1 has been found to interact with proteins that are involved in protein-quality control, for example, several heat-shock proteins such as Hsp70 (Shinder *et al.* 2001; Okado-Matsumoto and Fridovich 2002), Hsp40, αB-crystallin (Shinder *et al.* 2001), and Hsp27 (Okado-Matsumoto and Fridovich 2002) and E3 ligases such as dorfin (Niwa *et al.* 2002), NEDL1 (Miyazaki *et al.* 2004), and carboxy terminus of the Hsc70-interacting protein (Choi *et al.* 2004; Urushitani *et al.* 2004).

Abnormal expression of heat-shock proteins has been detected in mutant SOD1 mouse models. Increased expression of Hsp70 in mutant SOD1-expressing fibroblasts (Bruening *et al.* 1999) and of Hsp27 (also referred to as Hsp25) in spinal cord lysates of symptomatic $SOD1^{G93A}$ mice (Vleminckx *et al.* 2002) has been reported, but decreased expression of Hsp27 has also been found in motor neurons from symptomatic $SOD1^{G93A}$ mice (Maatkamp *et al.* 2004). Hsp70/Hsc70 were found in aggregates of mutant SOD1 in the motor neurons of symptomatic mutant SOD1 mice (Watanabe *et al.* 2001; Liu *et al.* 2005). These findings support the hypothesis that depletion of chaperone proteins might be responsible for the toxicity of mutant SOD1. Over-expression of Hsp70 in mutant SOD1 mice did not reverse the disease process (Liu *et al.* 2005), whereas activation of heat shock factor (HSF)-1, a transcription factor for heat-shock proteins, by administration of arimoclomol extended the life span of mutant SOD1 mice (Kieran *et al.* 2004). Such observations suggest that modulation of heat-shock responses might be an attractive strategy for treatment of motor neuron disease. Thus, it seems appropriate to elucidate the mechanism(s) of misregulation of heat-shock proteins that is linked to mutant SOD1-mediated toxicity, which remains poorly understood.

To uncover the properties of mutant SOD1 as they relate to protein-quality control, we investigated the proteins that interact with mutant SOD1 by immunoprecipitation (IP) and subsequent mass spectrometric (MS) analysis. We identified heat-shock protein 105 (Hsp105) as a novel mutant SOD1-interacting protein, and we detected this interaction in spinal cord extracts of mutant $SOD1^{G93A}$ transgenic mice. Levels of expression of Hsp105, which is detected in mouse motor neurons, were depressed in the spinal cords of $SOD1^{G93A}$ mice during disease progression, although levels of expression of other heat-shock protein rose. In addition, Hsp105 suppressed the aggregation of mutant SOD1 in cultured cells. Together, our findings indicate that raising levels of Hsp105 may alleviate the mutant SOD1-mediated toxicity.

Materials and methods

Plasmids

The coding region of human WT SOD1 cDNA was cloned into the expression vector pcDNA3.1(+) (Invitrogen, Carlsbad, CA, USA) and various mutations in SOD1 were generated (Oeda *et al.* 2001) by site-directed mutagenesis using a Mutan™-Super Express Km kit (Takara, Otsu, Japan), in accordance with the manufacturer's instruction. Then a FLAG tag was introduced at the carboxyl terminus of SOD1 and its mutant derivatives by PCR. A fragment of cDNA encoding mouse Hsp105 (Yasuda *et al.* 1995) was cloned into the pcDNA4/TO vector (Invitrogen).

Antibodies

The primary antibodies used for immunoblots or IP included anti-SOD1 antibody (Stressgen Biotechnologies, Victoria, BC, Canada), anti-FLAG antibody (M2; Sigma, St Louis, MO, USA), anti-β-actin antibody (Sigma), mouse anti-Hsp105 antibody (BD Biosciences, San Jose, CA, USA), anti-Hsp70 antibody (Santa Cruz Biotechnology, Santa Cruz, CA, USA), anti-Hsp27 antibody (Santa Cruz Biotechnology), and anti-β-galactosidase antibody (Chemicon, Temecula, CA, USA). For immunofluorescence staining, we used rabbit anti-Hsp105 antibody (Stressgen Biotechnologies) and SMI32 antibody (Sternberger Monoclonals, Baltimore, MA, USA). Secondary antibodies for immunoblots were anti-rabbit IgG conjugated with horseradish peroxidase (HRP; GE Healthcare, Piscataway, NJ, USA), anti-mouse IgG conjugated with HRP (GE Healthcare), and anti-goat IgG conjugated with HRP (Santa Cruz Biotechnology).

Culture and transfection of cells

Neuro2A and human embryonic kidney (HEK)293T cells were maintained in Dulbecco's modified Eagle's medium, supplemented with 10% fetal bovine serum, 100 IU/mL penicillin, 100 μg/mL streptomycin, and 2 mmol/L glutamine. Cells were transiently transfected with Lipofectamine™ 2000 (Invitrogen) according to the manufacturer's instruction. After 24 h, cells were harvested and cellular proteins were subjected to IP or immunoblotting.

Transgenic mice

Mutant (B6SJL-TgN [SOD1-G93A] 1Gur) and WT (B6SJL-Tg [SOD1] 2Gur/J) SOD1 transgenic mice were obtained from the Jackson Laboratory (Bar Harbor, ME, USA). Mice were genotyped by PCR with the following sense and antisense primers: 5′-CATCAGCCCTAATCCATCTGA-3′ and 5′-CGCGACTAACAAT-CAAAGTGA-3′, respectively. Mice were housed and treated in compliance with the 'Guidelines for Animal Experiments' of Kyoto University, Japan.

Preparation of lysates and IP of proteins

Lysates were prepared, on ice, from cells or tissue in lysis buffer (10 mmol/L Tris–HCl, pH 7.8, 1% Nonidet P-40, 0.15 mol/L NaCl, 1 mmol/L EDTA, and 10 μg/mL aprotinin). After centrifugation (21 600 *g*, 30 min, 4°C), the clarified supernatants were used for

© 2007 The Authors
Journal Compilation © 2007 International Society for Neurochemistry,

subsequent analysis unless specified. Protein concentrations were determined by Bradford's assay (Bio-Rad, Hercules, CA, USA). For IP, aliquots of 600 μg of protein in 1000 μL of lysis buffer were incubated for 12 h at 4°C with protein G-Sepharose (GE Healthcare). Then they were incubated with rabbit anti-SOD1 (3 μg) or mouse anti-FLAG antibodies (8.8 μg) or normal IgG for 1 h. The antibody–antigen complexes were then incubated with 10 μL of protein G-Sepharose for another hour. After immunoprecipitates had been washed five times with 1000 μL of lysis buffer, protein complexes were eluted with 15 μL of sample buffer for sodium dodecyl sulfate–polyacrylamide gel electrophoresis (SDS–PAGE) (0.125 mol/L Tris–HCl, pH 6.8, 4% SDS, 20% glycerol, 20 mmol/L dithiothreitol, and 0.002% bromo phenol blue) and immediately boiled for 5 min. Supernatants, after clarification by centrifugation, were loaded on a 2–15% polyacrylamide gradient gel (PAGmini; Daiichi Pure Chemicals, Tokyo, Japan) for SDS–PAGE.

Immunoblotting

Lysates prepared in lysis buffer or the whole tissue homogenates, which were prepared by homogenization of spinal cord with the equal volume of SDS sample buffer, were fractionated with SDS–PAGE, then transferred to a polyvinylidene difluoride membrane (Millipore Corporation, Bedford, MA, USA). Membranes were incubated with primary antibodies and appropriate HRP-conjugated secondary antibodies. Immunoreactive proteins on membranes were visualized with the enhanced chemiluminescence western blotting detection reagents (GE Healthcare).

MS

Proteins were identified by MS as described previously (Jensen *et al.* 1996). In brief, after SDS–PAGE, proteins were visualized by silver staining (PlusOne; GE Healthcare) and bands of proteins were excised from gels. After overnight in-gel digestions at 37°C of proteins with trypsin in a buffer that contained 50 mmol/L ammonium bicarbonate (pH 8.0) and 2% acetonitrile, molecular-mass analysis of tryptic peptides was performed by matrix-assisted laser desorption/ionization time-of-flight MS (MALDI-TOF/MS) with an Ultraflex MALDI-TOF/TOF system (Bruker Daltonics, Billerica, MA, USA). The acquired mass spectral data were queried against the National Center for Biotechnology Information non-redundant database using the Mascot (Matrix Science, London, UK) search engine with a peptide mass tolerance of 0.15 Da and allowance for up to two trypsin miscleavages.

Filter trap assay

Filtration of lysates through a cellulose acetate membrane (0.2-μm pores; Advantec, Dublin, CA, USA) was performed with a 96-well dot-blot apparatus (Bio-Rad) as described previously (Wang *et al.* 2002a) with minor modifications. In brief, HEK293T cells were cultured on 35-mm dishes to 70–80% confluence. Cells were co-transfected with 0.6 μg of empty vector or of plasmids encoding LacZ or Hsp105, together with 1 μg of plasmid encoding SOD1^{G93A}-FLAG. After incubation for 48 h, cells were harvested with phosphate-buffered saline (PBS) and briefly sonicated. Lysates were centrifuged at 800 *g* for 10 min at 4°C and the concentrations of proteins in the supernatants were determined. Aliquots of 200 μg of protein in 400 μL of lysis buffer (PBS, 1% SDS) were gently vacuum-filtered through a membrane. Membranes were washed twice with tris-buffered saline-0.05% Tween20 and analyzed by immunoblotting.

Immunofluorescence staining

For immunofluorescence staining, mice were deeply anesthetized with pentobarbital and perfused transcardially with 4% *p*-formaldehyde in PBS. The lumbar spinal cord was dissected out, fixed overnight in 4% *p*-formaldehyde in PBS, and cryoprotected with 30% sucrose in PBS before freezing. Ten-micron cryosections were mounted on slides. After blocking with blocking buffer (5% normal goat serum and 0.3% Triton X-100 in PBS) for half an hour at 25°C, the sections were incubated overnight at 4°C with a mixture of mouse SMI32 antibody (1 : 4000) and rabbit anti-Hsp105 antibody (1 : 100). Bound antibodies were detected with Alexa Fluor 488-conjugated anti-rabbit IgG and Alexa Fluor 594-conjugated anti-mouse IgG antibodies (1 : 1000; Molecular Probes, Eugene, OR, USA). Double-immunostained fluorescent images were recorded with a Leica DMRXA2 confocal microscope (Leica, Wetzlar, Germany).

Statistical analysis

Signals on films were quantified with NIH image software (National Institutes of Health, Bethesda, MD, USA). Statistical significance was assessed by one-way ANOVA followed by Scheffe's *post hoc* test using the KaleidaGraph program (Synergy Software, Reading, PA, USA). Statistical significance was set at a probability value of less than 0.05.

Results

Identification of proteins that interact with mutant SOD1 in Neuro2A cells by MALDI-TOF/MS

We attempted to identify proteins that interact specifically with ALS-associated mutant SOD1 proteins by IP and subsequent MS analysis, as illustrated in Fig. 1a. We transfected Neuro2A cells transiently with plasmids that encoded SOD1^{WT}-FLAG, SOD1^{G85R}-FLAG, or SOD1^{G93A}-FLAG. After 24 h, proteins in lysates from transfected Neuro2A cells were immunoprecipitated with anti-FLAG antibody or control mouse IgG. The immunoprecipitates were fractionated by SDS–PAGE, which was followed by silver staining (Figs 1b and c). We considered all bands in lanes 1, 5, and 6 to represent non-specifically interacting proteins, as they were generated in the absence of mutant SOD1 (lane 1), in the presence of control IgG (lane 5), or in the absence of antibody for IP (lane 6). We detected bands of a protein of ~19 kDa in lanes 2 and 4 and of a protein of ~18 kDa in lane 3, each of which was confirmed to be exogenous SOD1-FLAG by immunoblotting (data not shown). We identified two specific bands of proteins of approximately 70 kDa (p70) and 105 kDa (p105), respectively, that were visualized exclusively in both lanes 3 and 4 (Figs 1b and c). These two bands were excised and subjected to MALDI-TOF/MS analysis. A search for a protein similar to p70 gave 28 matches (*m/z*; 1081.53, 1197.57, 1199.59,

© 2007 The Authors

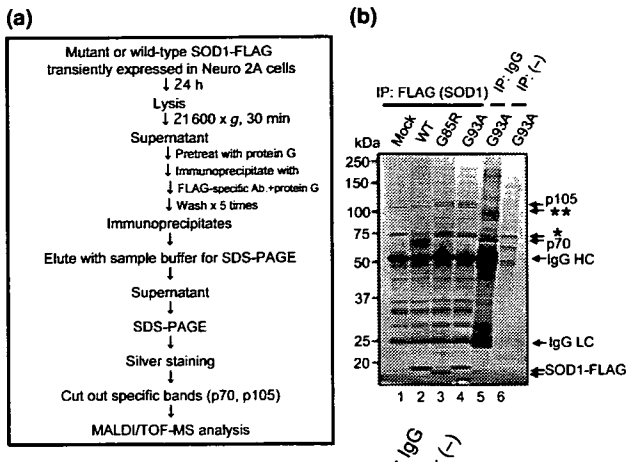

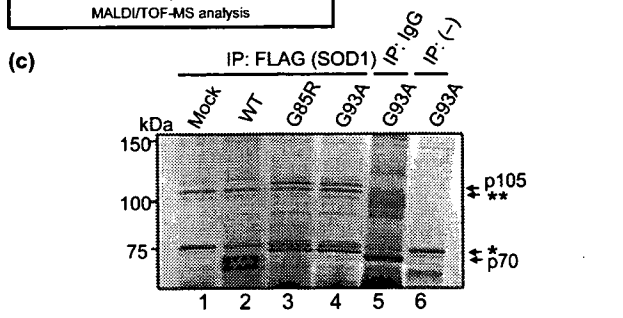

(d)

Band fraction	Protein name		Sequence coverage (%)
p105	heat-shock protein 105	(gi17390885)	13.7
p70	heat-shock cognate protein 70	(gi42542422)	56.9

Fig. 1 Identification of amyotrophic lateral sclerosis-associated mutant superoxide dismutase 1 (SOD1) -interacting proteins by sodium dodecyl sulfate–polyacrylamide gel electrophoresis (SDS–PAGE) and matrix-assisted laser desorption/ionization time-of-flight mass spectrometry (MALDI-TOF/MS) analysis. (a) Scheme for the experiments designed to identify proteins that interact with mutant SOD1. (b and c) Mutant SOD1-interacting proteins, as visualized by silver staining. Arrows indicate interacting proteins (p70 and p105 in lanes 3 and 4), IgG heavy chain (HC), IgG light chain (LC), and FLAG-tagged human SOD1 (lanes 2–4). The G85R mutant form of SOD1 migrates faster than the wild type (lane 3). Asterisks (* and **) denote non-specific bands. Figure 1c shows an enlarged view of the region of the photograph that includes proteins of 50–150 kDa proteins in Fig. 1b. Two proteins that interacted specifically with mutant SOD1 are apparent (p70 and p105; lanes 3 and 4). The mobilities of these correspond to molecular masses of ~70 kDa (p70) and ~105 kDa (p105), respectively. These two bands were excised and were prepared for MS analysis. (d) MS analysis of the excised proteins in Fig. 1c. Percentage sequence coverage of each protein is shown.

1228.55, 1235.54, 1252.59, 1253.56, 1391.67, 1410.62, 1480.71, 1481.77, 1487.67, 1616.76, 1649.78, 1653.81, 1659.84, 1691.73, 1787.97, 1805.86, 1837.97, 1952.04, 1981.99, 2206.09, 2260.13, 2514.34, 2774.37, 2911.63, and 2997.52) with Hsc70 (heat-shock cognate protein 70) with 56.9% sequence coverage. In the analysis of p105, although the sequence coverage (13.7%) was lower than that of p70, 10 peaks of the theoretical mass fingerprint of Hsp105 (heat-shock protein 105) matched with the mass observed (*m/z*; 1133.56, 1321.62, 1388.67, 1479.70, 1481.75, 1487.75, 1562.77, 1637.78, 2035.13, and 2111.03) (Fig. 1d).

Those data highly suggested Hsc70 was interacted with mutant SOD1 proteins as previously reported (Shinder *et al.* 2001). More interestingly, the MS analysis also suggested a novel interaction between Hsp105 and mutant SOD1, which required further confirmation.

Interaction of mutant SOD1 with Hsp105 both in cultured neuroblastoma cells and in mouse spinal cord

Having identified a possible novel interaction between Hsp105 and mutant SOD1, we decided to investigate the role of Hsp105 in the toxicity of mutant SOD1. We first confirmed the interaction between different mutant forms of SOD1 and endogenous Hsp105 in Neuro2A cells. We transiently transfected Neuro2A cells with plasmids that expressed FLAG-tagged SOD1 (WT) and its mutant derivatives (D96N, D90A, G85R, and G93A). Then we immunoprecipitated proteins in lysates with anti-FLAG antibody. Immunoprecipitated proteins were examined by immunoblotting for the presence of Hsp105 (Fig. 2a, upper panel) and SOD1-FLAG (Fig. 2a, second panel). Only G85R and G93A mutant forms of SOD1, which cause motor neuron disease as a dominant trait, interacted with Hsp105; WT SOD1, D96N, and D90A mutant forms of SOD1 did not. The lack of interaction of $SOD1^{D90A}$ and $SOD1^{D96N}$ with Hsp105 suggested the lower toxicity of those mutants. This observation reflects the facts that $SOD1^{D90A}$ causes motor neuron disease as a mainly recessive trait (Andersen *et al.* 1996) and that the D96N mutation has been reported as a non-disease-associated mutation, though controversial (Hand *et al.* 2001; Parton *et al.* 2001).

Next, we used mouse tissue to examine whether the interaction between mutant SOD1 and Hsp105 might occur *in vivo*. Lysates of spinal cord and of liver cells from non-transgenic, $SOD1^{WT}$ and $SOD1^{G93A}$ mice were treated with anti-SOD1 antibody and immunoprecipitates were examined for the presence of Hsp105 (Fig. 2b, upper panel) and SOD1 (Fig. 2b, second panel). In spinal cord extracts, $SOD1^{G93A}$ co-immunoprecipitated with Hsp105 (lane 3), while $SOD1^{WT}$ interacted with Hsp105 at a lower level (lane 2). No evident interaction between SOD1 and Hsp105 was detected in liver, a tissue that is not affected in ALS.

Although it has been reported that Hsp105 is expressed in brain at higher levels (Lee-Yoon *et al.* 1995; Yasuda *et al.* 1995), the cell type(s) that expresses Hsp105 in the spinal cord is unknown. We examined whether Hsp105 is expressed in motor neurons by immunofluorescence staining of spinal cord from non-transgenic mice. Motor neurons that were immunostained with the SMI32 antibody were immunopositive for Hsp105 (Fig. 2c, arrowheads), whereas non-motor neurons were also stained with anti-Hsp105 antibody (Fig. 2c, arrows). Within the motor neurons, Hsp105 was mainly localized in the cytoplasm, as is SOD1.

© 2007 The Authors
Journal Compilation © 2007 International Society for Neurochemistry,

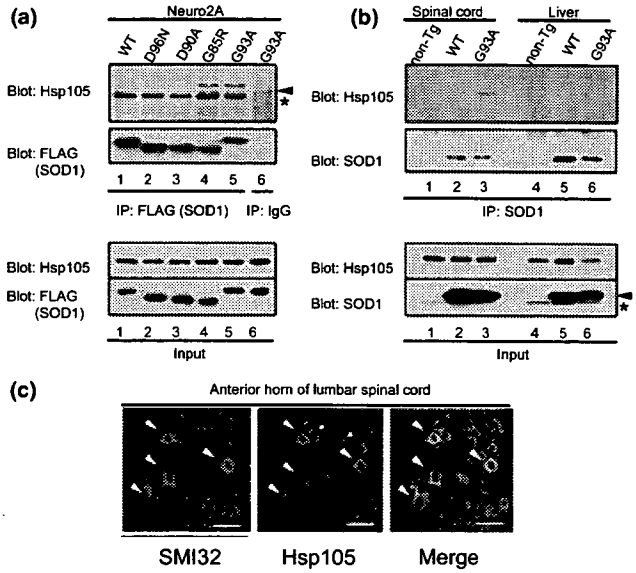

Fig. 2 Hsp105 interacts with mutant superoxide dismutase 1 (SOD1) both in neuroblastoma cells in culture and in mouse spinal cord. (a) Lysates of Neuro2A cells that had been transiently transfected with FLAG-tagged wild-type (WT, lane 1) or mutant SOD1 expression vector (lanes 2–6) were immunoprecipitated with anti-FLAG antibody (lanes 1–5) or normal IgG (lane 6). Immunoprecipitates were analyzed by immunoblotting specific for Hsp105 (top panel) or FLAG (second panel). The arrowhead and the asterisk indicate Hsp105 and non-specific bands, respectively. Ten micrograms (as protein) of each lysate that was subjected to immunoprecipitation were analyzed by immunoblotting (third and fourth panels). (b) Proteins in extracts of spinal cord and of liver from non-transgenic, SOD^{WT}, and SOD^{G93A} mice were immunoprecipitated with anti-SOD1 antibody. Blots were probed for Hsp105 (top panel) or SOD1 (second panel). Eight micrograms (as protein) of the lysate used for immunoprecipitation were immunoblotted with indicated antibodies (third and fourth panels). The arrowhead and the asterisk indicate human SOD1 and endogenous mouse SOD1, respectively. (c) Confocal fluorescence micrographs of lumbar spinal cord from a non-transgenic mouse after double staining with SMI32 antibody (left panel) and anti-Hsp105 antibody (middle panel), and the merged image (right panel). Arrowheads indicate motor neurons that immunoreacted with both antibodies. Arrows indicate non-motor neurons that immunoreacted with only anti-Hsp105 antibody. Hsp105 was mainly localized in the cytoplasm of motor neurons. Scale bars: 50 μm.

Decreased expression of Hsp105 during disease progression in $SOD1^{G93A}$ mice

Heat-shock responses such as increased levels of Hsp27, Hsp70, and Hsp90 have been reported in the spinal cords of mutant SOD1 transgenic mice (Vleminckx *et al.* 2002; Liu *et al.* 2005). To examine changes in levels of heat-shock proteins, including Hsp105, we performed immunoblotting analyses of Hsp105, Hsp70, and Hsp27 in the brain, spinal cord, and liver of SOD^{WT} mice at 5 months of age and in $SOD1^{G93A}$ mice at two different ages. By contrast to levels of other heat-shock proteins, the level of Hsp105 was lower in the spinal cord of symptomatic $SOD1^{G93A}$ mice (4-months old) than in that of pre-symptomatic $SOD1^{G93A}$ mice (2.5-months old) (Fig. 3a, upper panel, lanes 5 and 6).

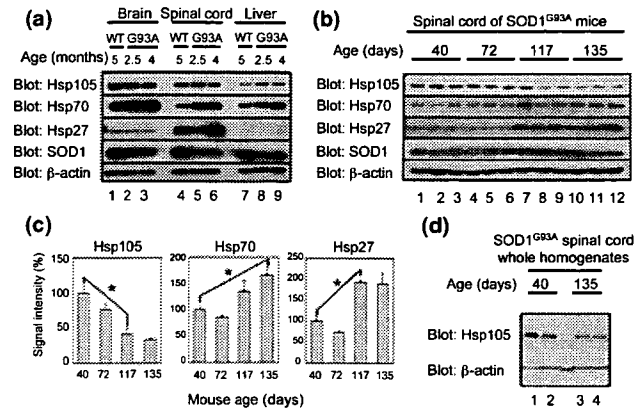

Fig. 3 Decreases in the levels of expression of Hsp105 in the spinal cord during disease progression in superoxide dismutase 1 ($SOD1^{G93A}$) mice. (a) Immunoblotting analysis of Hsp105, Hsp70, and Hsp27 in the brain, spinal cord, and liver of $SOD1^{WT}$ and $SOD1^{G93A}$ mice at two different ages, as indicated. A total of 15 μg of protein was loaded in each lane. The level of Hsp105 was lower in the spinal cord of symptomatic $SOD1^{G93A}$ mice (4 months; lane 6) than in pre-symptomatic $SOD1^{G93A}$ mice (2.5 months; lane 5) (upper panel). The same membrane was immunoprobed for Hsp70 (second panel), Hsp27 (third panel), hSOD1 (fourth panel), and β-actin as a loading control (fifth panel). (b) Immunoblotting analysis of Hsp105, Hsp70, and Hsp27 in the spinal cord of early pre-symptomatic (40-day old), late pre-symptomatic (72-day old), symptomatic (117-day old), and end-stage (135-day old) $SOD1^{G93A}$ mice ($n = 3$ at each time point). A total of 15 μg of protein was loaded in each lane. Membranes were blotted with the indicated antibodies. (c) Densitometric analysis of the immunoblots shown in Fig. 3b. Results are expressed relative to the intensity of signals for 40-day-old mice, which were normalized to 100%. Values are expressed as means ± SE. Asterisks indicate significant difference ($p < 0.05$). (d) Immunoblotting analysis of Hsp105 using whole homogenates from the spinal cord of $SOD1^{G93A}$ mice at pre-symptomatic (40-day old) and end-stage (135-day old). A total of 40 μg of protein was loaded in each lane. Membranes were blotted with the indicated antibodies.

To investigate the level of expression of heat-shock proteins in $SOD1^{G93A}$ mouse spinal cord in grater detail, we performed immunoblotting analysis of Hsp105, Hsp70, and Hsp27 in spinal cords from early pre-symptomatic (40-day old), late pre-symptomatic (72-day old), symptomatic (117-day old), and end-stage (135-day old) $SOD1^{G93A}$ mice (Fig. 3b). Decreased levels of Hsp105 were apparent as early as late pre-symptomatic stage (72 days). However, the decrease did not reach statistical significance. The expression of Hsp105 was significantly depressed as the disease progressed, whereas the levels of expression of both Hsp70 and Hsp27 were elevated at the symptomatic stage and the end-stage (Figs 3b and c). Semi-quantitative immunoblotting confirmed ≈50% decrease of level of Hsp105 in the spinal cord lysates from end-stage $SOD1^{G93A}$ mice (135-day old)

© 2007 The Authors

compared with ones from pre-symptomatic mice (40-day old) (Fig. S1).

To investigate whether the decrease in Hsp105 level was associated with the recruitment of Hsp105 to NP-40-insoluble fraction, we performed immunoblotting analysis using whole homogenates from the spinal cord of SOD1^{G93A} mice at pre-symptomatic and end-stage. Whole homogenates were prepared by homogenizing mouse spinal cords with sample buffer for SDS–PAGE and analyzed by immunobloting. The significant decrease in Hsp105 level at end-stage was still observed (Fig. 3d), suggesting that the decrease of Hsp105 was unlikely to be due to the sequestration of Hsp105 into the insoluble fraction.

Inhibition by Hsp105 of the formation of mutant SOD1-containing aggregates in cultured cells

Intracellular inclusions that are strongly immunopositive for SOD1 are found in the motor neurons of mutant SOD1 transgenic mice and in human ALS patients with a mutation in SOD1 (Bruijn *et al.* 1998). These misfolded, detergent-resistant protein aggregates are considered to be relevant to progression of the disease as increased accumulation of these aggregates has been observed in symptomatic mutant SOD1 mice (Bruijn *et al.* 1997; Johnston *et al.* 2000; Wang *et al.* 2002b). To determine whether Hsp105 can suppress the formation of mutant SOD1-containing aggregates, we studied the effects of over-expression of Hsp105 on the aggregation of mutant SOD1 in a filter trap assay. We co-transfected HEK293T cells with an SOD1^{G93A}-FLAG expression vector together with the empty vector, a vector that encoded β-galactosidase or a vector that encoded Hsp105. After 48 h, we harvested the cells and processed them for the filter trap assay. We examined the SDS-insoluble SOD1 aggregates that were retained on cellulose acetate membranes by immunoblotting. Hsp105 significantly suppressed the aggregation of mutant SOD1 (Fig. 4, upper panel). Moreover, the level of expression of SOD1^{G93A} in HEK293T cells was very similar in all the samples examined. Taken together, the results indicate that Hsp105 reduced the level of mutant SOD1-containing aggregates by inhibiting the formation of aggregates rather than by facilitating their degradation.

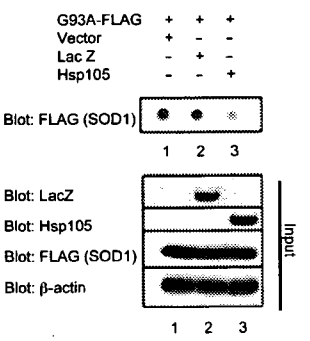

Fig. 4 Hsp105 suppressed the aggregation of mutant superoxide dismutase 1 (SOD1) in cultured cells. HEK293T cells were co-transfected with an SOD1^{G93A}-FLAG expression vector together with the empty vector, an expression vector for β-galactosidase (LacZ), or an expression vector for Hsp105, as indicated. Lysates were analyzed by the filter trap assay with subsequent immunoblotting with anti-FLAG antibody, as described in the text (upper panel). The experiment was repeated three times with essentially the same results. Lower panels show the results of analysis of input in the filter trap assay.

Discussion

In the present study, we have identified a novel interaction between Hsp105 and mutant SOD1 both in cultured cells and in a mouse model. Although the involvement of other heat-shock proteins has been demonstrated in mutant SOD1-mediated toxicity, we demonstrated, for the first time to our knowledge, a decrease in the level of expression of Hsp105, specifically, from the symptomatic to the end-stage of disease in the mutant SOD1 mouse model unlike other heat-shock proteins (Fig. 3). This result might be explained by several properties of Hsp105, which make it uniquely different from Hsp70, a major molecular chaperone that is involved in the folding of newly synthesized and misfolded proteins, even though these heat-shock proteins are structurally similar.

Hsp105, which is a constitutively expressed 105-kDa protein whose synthesis is enhanced by the various stress stimuli, is concentrated in the brain, which suggests a specific role for Hsp105 in stress responses within the nervous system (Lee-Yoon *et al.* 1995; Yasuda *et al.* 1995). Hsp105 exhibits significant homology at the amino acid level to Hsp70, in particular in the amino-terminal ATPase domain. The chaperone activity of Hsp70/Hsc70 (Hsp70s) is controlled by a series of ATP-dependent reaction cycles that consist of the binding of ATP, hydrolysis of ATP, and nucleotide exchange (Buchberger *et al.* 1995; McCarty *et al.* 1995; Rudiger *et al.* 1997). By contrast, Hsp105 does not require ATP to prevent the aggregation of denatured proteins (Yamagishi *et al.* 2003), but it does act as a nucleotide-exchange factor for Hsp70s, which suggests a role for Hsp105 in supporting the functions of Hsp70s (Dragovic *et al.* 2006; Raviol *et al.* 2006). Hsp105 binds to denatured proteins *in vitro* and maintains these proteins in a folding-competent state rather than refolding them itself (Oh *et al.* 1997, 1999; Yamagishi *et al.* 2003). Thus, Hsp105 might function not only in collaboration with Hsp70s but also as a substitute for Hsp70s under severe stress condition, when cellular supplies of ATP have been markedly depleted. In motor neurons that express mutant SOD1, Hsp70s might not be functional, since the level of cellular ATP is likely to be low as a result of consumption by Hsp70s and the ubiquitin-proteasome system. This scenario might explain the failure of over-expression of Hsp70 to mitigate the toxicity of mutant SOD1 in mice (Liu *et al.* 2005). Therefore, rather than

© 2007 The Authors
Journal Compilation © 2007 International Society for Neurochemistry,

Hsp70, Hsp105 might be a promising candidate for a suppressor of mutant SOD1 toxicity.

We observed the decreased level of Hsp105 in spinal cord of $SOD1^{G93A}$ mice as disease progressed (Fig. 3b) and further confirmed ≈50% decrease in Hsp105 levels at end-stage by semi-quantitative immunoblotting analysis (Fig. S1). This result might partly reflect the loss of motor neurons, which contain abundant Hsp105 proteins. However, considering the facts that lumbar spinal cord sections of $SOD1^{G93A}$ mice at the end-stage show approximately 50% loss of motor neurons (Kostic *et al.* 1997; Bendotti and Carri 2004) and that Hsp105 is expressed not only in motor neurons but also in non-motor neurons (Fig. 2c), it is less likely that Hsp105 was decreased as a consequence of only motor neuronal loss. Immunoblotting analysis of whole spinal cord homogenates also revealed the decreased level of Hsp105 in spinal cord of $SOD1^{G93A}$ mice (Fig. 3d). Therefore, although a fraction of Hsp105 might be lost in aggregates, a significant part of Hsp105 is likely to be consumed or degraded by interacting with mutant SOD1.

Consistent with the reports of the ability of Hsp105 to maintain denatured proteins in a folding-competent state (Oh *et al.* 1997, 1999; Yamagishi *et al.* 2003), we have shown that Hsp105 is able to suppress the formation of aggregates of mutant SOD1 in cultured cells. Mutant SOD1-containing aggregates immunoreact strongly with antibodies raised against ubiquitin, and this phenomenon is common to all mutant SOD1-expressing mouse models (Bruijn *et al.* 1998; Wang *et al.* 2003; Jonsson *et al.* 2004) and human patients (Bruijn *et al.* 1998; Kato *et al.* 2000; Watanabe *et al.* 2001). These findings, together with decreased expression of Hsp105 in symptomatic $SOD1^{G93A}$ mice, suggest that depletion of Hsp105 might contribute to the process of motor neuron degeneration through the accumulation of aggregates of misfolded mutant SOD1.

Hsp105 is essential for cell survival in eukaryotes. Combined deletion in yeast cells of the *SSE1* and *SSE2* genes, which encode members of the Hsp105/110 family, is lethal (Raviol *et al.* 2006). Moreover, recessive mutations in the *SIL1* gene, whose product functions as a nucleotide-exchange factor for the protein of the Hsp70 family, Bip (GRP78), are responsible for Marinesco–Sjögren syndrome, which is characterized by cerebellar atrophy with degeneration of Purkinje and granule cells (Anttonen *et al.* 2005; Senderek *et al.* 2005). Combined with recent reports that Hsp105 is a nucleotide-exchange factor for Hsp70s, these findings provide a link between a functional deficit in a nucleotide-exchange factor for the proteins of the Hsp70 family and neurodegeneration. With respect to neuronal survival, over-expression of Hsp105 has an anti-apoptotic effect in cultured neuronal PC12 cells (Hatayama *et al.* 2001). Hsp105 suppresses apoptosis in a cell culture model of polyglutamine disease, a neurodegenerative disease caused by the toxicity that is derived from a misfolded mutant protein (Ishihara *et al.* 2003). Moreover, we observed Hsp105 prevented caspase-activation induced by proteasomal inhibition with lactacystin in neuroblastoma cell line (Yamashita *et al.*, unpublished data). These results suggest that enhanced expression of Hsp105 might contribute to prevention of motor neuron degeneration through its anti-apoptotic property.

Increased expression of Hsp70s in spinal cord lysates from our $SOD1^{G93A}$ mice and from $SOD1^{G85R}$ mice (Liu *et al.* 2005), together with the impaired heat-shock response of Hsp70 in mutant SOD1-expressing motor neurons (Batulan *et al.* 2003), suggests the enhanced expression of Hsp70s in glial cells. In accordance with this hypothesis, elevated levels of Hsp27 were also observed in the glial cells of $SOD1^{G93A}$ mice (Vleminckx *et al.* 2002). However, this scenario does not apply to Hsp105, because (i) continuous decreases in levels of Hsp105 were observed throughout the course of the disease and (ii) Hsp105 is concentrated in neurons and not in glial cells (Hylander *et al.* 2000). Absence of the induction of expression of Hsp105 in non-neuronal glial cells might exacerbate the toxicity of mutant SOD1 as the toxicity of the mutant protein to motor neurons is non-cell autonomous (Clement *et al.* 2003; Boillee *et al.* 2006).

Over-expression of Hsp70 did not ameliorate the condition of mutant SOD1 mice (Liu *et al.* 2005). By contrast, the pharmacological activation of HSF-1, a transcription factor for heat-shock proteins, extended the life span of mutant SOD1 mice by enhancing the expression of Hsp70s and Hsp90. In the cited study, the level of Hsp105 was not measured (Kieran *et al.* 2004). In spinal and bulbar muscular atrophy mouse model, in which accumulation of misfolded polyglutamine protein causes motor neuron degeneration, pharmacological induction of the expression of HSF-1 by geranylgeranylacetone alleviated polyglutamine-mediated motor neuron disease and activation of HSF-1 was shown to induce the expression of Hsp70, Hsp90, and Hsp105 but not of Hsp27, Hsp40, and Hsp60 (Katsuno *et al.* 2005). In view of our observation of depleted supplies of Hsp105 in $SOD1^{G93A}$ mice, a requirement for enhanced synthesis of Hsp70s, Hsp90, and Hsp105 in both neuronal cells and non-neuronal neighboring cells might be crucial for the mitigation of mutant SOD1-mediated toxicity.

Acknowledgements

The authors thank Dr K. Ishihara (RIKEN Brain Science Institute) for a critical review of the original manuscript, Ms K. Odan (Kyoto University) for technical assistance, and Drs K. Uemura and A. Kuzuya (Kyoto University) for kind advice. This work was supported by the Nakabayashi Trust for ALS Research; the Ministry of Education, Culture, Sports, Science and Technology of Japan; the Ministry of Health, Labor and Welfare of Japan; the Smoking Research Foundation; Philip Morris USA Inc. and Philip Morris International.

© 2007 The Authors